

f-MODE INTERACTIONS WITH THIN FLUX TUBES: THE SCATTERING MATRIX

S. M. HANASOGE,¹ A. C. BIRCH² T. J. BOGDAN,³ AND L. GIZON⁴

Received 2007 November 13; accepted 2008 January 18

ABSTRACT

We calculate the scattering effects associated with the interaction of a surface gravity or *f*-mode with a thin magnetic flux tube embedded in a realistically stratified medium. We find that the dominant scattered wave is an *f*-mode with amplitude and phase of 1.17% and around 50° relative to the incident wave, compared to the values of 0.13% and 40° estimated from observations. The extent of scattering into high-order acoustic *p*-modes is too weak to be accurately characterized. We recover the result that the degree of scattering is enhanced as (1) the frequency of the incident wave increases and (2) the flux tube becomes magnetically dominated.

Subject headings: hydrodynamics — Sun: helioseismology — Sun: interior — Sun: oscillations — waves

Online material: color figures

1. INTRODUCTION

A problem of considerable interest and more recently controversy relates to the influence of magnetic fields on acoustic waves in the near-surface regions of the Sun. In these subphotospheric magnetic regions, the ratio of magnetic to gas pressure could be very close to unity (e.g., McIntosh et al. 2003; McIntosh & Jefferies 2006), leading to the contention that magnetic field effects are systematic and significant. Mode conversion (e.g., Spruit & Bogdan 1992; Barnes & Cally 2000) is a phenomenon commonly invoked to describe magnetohydrodynamic (MHD) wave interactions; from one acoustic mode to another, from acoustic modes to Alfvén waves, and so on, it is estimated that acoustic energy is redistributed, contributing perhaps to *p*-mode absorption observed in sunspots (Braun 1995).

Thin flux tubes are important building blocks of solar magnetic activity, intimately tied to studies of the solar photospheric dynamo (e.g., Cattaneo 1999) and flux emergence (e.g., Cheung et al. 2006). One way of deconstructing the structure and dynamics of thin flux tubes is through experimental analyses of changes in the statistics of the wave field in the vicinity of these magnetic features. Applying techniques of time-distance helioseismology (Duvall et al. 1993), Duvall et al. (2006) estimated the phase and amplitude of the scattered *f*-modes from observations of thousands of isolated, small magnetic features. These parameters contain the scattering properties of an “average” flux tube, giving us an insight into the nature of these flux tubes.

However, one must apply caution when invoking causative mechanisms to explain these statistics, taking care to understand the nature of wave scattering in the presence of magnetic fields (e.g., Spruit & Bogdan 1992; Bogdan & Cally 1995; Bogdan et al. 1996; Barnes & Cally 2000). Once a sound theoretical basis is formed, observations characterizing the extent of scatter can be used to place constraints on theories of the structure and dynamics of flux tubes.

In an attempt to construct an analytical framework to decipher the nature of wave interaction with magnetic regions, Bogdan et al. (1996) model a magnetic flux concentration in the thin tube limit (e.g., Spruit 1981) embedded in a truncated polytrope. The flux tube is assumed to be thin enough that variations across its interior are neglected; moreover, the tube must be a subwavelength feature and the radius small in comparison to the pressure scale height. The parameters of the polytrope are selected so as to mimic the solar subphotospheric layers as closely as possible; the polytrope itself is truncated a little below the photosphere because the rapidly diminishing density makes the thin tube approximation inapplicable very close to the surface. These simplifying assumptions reduce the generality of the results presented here, and in fact, direct numerical solvers might appear to be a more attractive proposition. However, while numerical simulations can undoubtedly be employed to address a broader range of questions, it is also important to develop an analytical treatment of a comparable situation, as we attempt to do in this paper. Such results serve not only as benchmarks for direct computations of these phenomena but also assist us in developing a theoretical appreciation of MHD-wave interactions.

Bogdan et al. (1996) have demonstrated that the dominant flux tube mode is the kink mode and that the *f*-mode couples strongly with the flux tube. Moreover, the measurements of Duvall et al. (2006) are for *f*-modes. Consequently, the focus of this paper will be to quantify the interaction between an incoming *f*-mode and the resulting kink mode exhibited by the flux tube. In § 2 we describe the model in greater detail, followed by a discussion of the method we apply to extract the scattering coefficients in § 3. The theoretical values of the phase and amplitude of the scattered *f*-mode are compared with those obtained by Duvall et al. (2006; also see Appendix B). We also demonstrate that the scattering process is predominantly restricted to *f*-*f*, while the *f*-*p* conversions are very weak. We conclude with a summary of our calculations and a discussion of the relevance and importance of these results in § 4.

2. THE MODEL

The background structure in this calculation, adapted from Bogdan et al. (1996), is an adiabatically stratified, truncated polytrope with index $m = 1.5$, gravity $g = -2.775 \times 10^4 \text{ cm s}^{-2} \hat{z}$, reference pressure $p_0 = 1.21 \times 10^5 \text{ g cm}^{-1} \text{ s}^{-2}$, and reference density

¹ W. W. Hansen Experimental Physics Laboratory, Stanford University, Stanford, CA 94305.

² Colorado Research Associates Division, NorthWest Research Associates, Inc., 3380 Mitchell Lane, Boulder, CO 80301.

³ Space Environment Center, National Oceanic and Atmospheric Administration, 325 Broadway, Boulder, CO 80305.

⁴ Max-Planck-Institut für Sonnensystemforschung, Max-Planck-Strasse 2, 37191 Katlenburg-Lindau, Germany.

$\rho_0 = 2.78 \times 10^{-7} \text{ g cm}^{-3}$, such that the pressure and density variations are given by

$$p(z) = p_0 \left(-\frac{z}{z_0} \right)^{m+1}, \quad (1)$$

$$\rho(z) = \rho_0 \left(-\frac{z}{z_0} \right)^m. \quad (2)$$

We utilize a right-handed cylindrical coordinate system in our calculations, with coordinates $\mathbf{x} = (r, \theta, z)$ and corresponding unit vectors $(\hat{\mathbf{r}}, \hat{\boldsymbol{\theta}}, \hat{\mathbf{z}})$. The photospheric level of the background model is at $z = 0$, with the upper boundary placed at a depth of $z_0 = 392 \text{ km}$. Following Barnes & Cally (2000) we introduce a lower boundary at a depth of 98 Mm. The displacement potential $\Psi(\mathbf{x}, t)$ describing the oscillation modes (t is time) is required to enforce zero Lagrangian pressure perturbation boundary conditions at both boundaries. This upper boundary condition is reflective in nature and, therefore, possibly not very realistic. In comparison, the formalism that Crouch & Cally (1999) adopt in treating upward-propagating waves at the boundary appears to be more fitting, but is rather difficult to implement. While the choice of “good” boundary conditions is an important issue, that of incorporating the effects of the ubiquitous magnetic field that pervades the atmospheric layers is an equally, if not more important aspect (e.g., Crouch & Cally 1999; Hanasoge 2008). Moreover, the thin flux tube approximation rapidly breaks down as one proceeds higher into the atmosphere. As a first step, we have therefore chosen to (1) truncate the background model a little below the photosphere and (2) adopt simplistic boundary conditions, thereby not having to deal with the uncomfortably complex physics of the atmosphere. The incoming f -mode, a plane wave, when expanded in cylindrical coordinates (e.g., Bogdan 1989; Gizon et al. 2006) has a displacement eigenfunction, Ψ_{inc} , of the form

$$\Psi_{\text{inc}} = \sum_{m=-\infty}^{\infty} i^m J_m(k_0^p r) \Phi_p(\kappa_0^p; s) e^{i(m\theta - \omega t)}, \quad (3)$$

where

$$\Phi_p(\kappa_n^p; s) = s^{-1/2 - \mu} N_n \left[\zeta_n^p M_{\kappa_n^p, \mu} \left(\frac{s\nu^2}{\kappa_n^p} \right) + M_{\kappa_n^p, -\mu} \left(\frac{s\nu^2}{\kappa_n^p} \right) \right]. \quad (4)$$

In equations (3) and (4), we have introduced a slew of new symbols:

$$\mu = \frac{m-1}{2}, \quad \nu^2 = \frac{m\omega^2 z_0}{g}, \quad k_n^p = \frac{\nu^2}{2\kappa_n^p z_0}, \quad (5)$$

ω the angular frequency of oscillation, $s = -z/z_0$, $J_m(w)$ the Bessel function of order m and argument w , and $M_{\kappa, \mu}(w)$ the Whittaker function (e.g., Whittaker & Watson 1980) with indices κ, μ and argument w . The eigenvalue $\kappa_n^p > 0$ and constant ζ_n^p characterizing the mode are obtained through the procedure described in Appendix A. The $n = 0$ mode corresponds to the surface gravity or f -mode, while $n > 0$ represents the acoustic p_n -mode. The term N_n is the normalization constant for the mode, defined as

$$N_n = \left\{ \int_1^\infty \left[\zeta_n^p M_{\kappa_n^p, \mu} \left(\frac{\nu^2 s}{\kappa_n^p} \right) + M_{\kappa_n^p, -\mu} \left(\frac{\nu^2 s}{\kappa_n^p} \right) \right]^2 ds \right\}^{-1/2}. \quad (6)$$

2.1. Flux Tube

Applying the approximations listed in § 2 of Bogdan et al. (1996), a thin flux tube carrying a magnetic flux of $\Phi_f =$

$3.88 \times 10^{17} \text{ Mx}$, with plasma- $\beta = 1$ everywhere inside the tube, is placed in the polytrope. The thin flux tube approximation,

$$b(s) \approx \sqrt{\frac{8\pi p(s)}{1+\beta}}, \quad \pi R^2(s) \approx \frac{\Phi_f}{b(s)}, \quad (7)$$

where $b(s)$ and $R(s)$ are the magnetic field and the radius of the tube at depth s , is shown to be accurate to better than a percent in the truncated polytrope situated below $z = -z_0$ or $s = 1$ (Bogdan et al. 1996). Note that the magnetic flux associated with the tube is held constant over different values of β , thereby resulting in different $b(s)$ and $R(s)$.

2.2. Oscillations of the Tube: The Kink Mode

Horizontal motions of the flux tube created by the impinging modes [whose displacement potential is given by $\Psi(\mathbf{x}, t)$] in the direction of the wavevector are described by $\xi(s, t)$ (e.g., Bogdan et al. 1996), a solution to the differential equation

$$\left[z_0 \frac{\partial^2}{\partial t^2} - \frac{2gs}{(1+2\beta)(m+1)} \frac{\partial^2}{\partial s^2} - \frac{g}{1+2\beta} \frac{\partial}{\partial s} \right] \xi = \frac{2(1+\beta)}{1+2\beta} z_0 \frac{\partial^3 \Psi}{\partial x \partial t^2}, \quad (8)$$

where $x = r \cos \theta$. Following Bogdan et al. (1996) we define $\xi_\perp = -i\tilde{\xi}(s)$, where $\xi(s, t) = \tilde{\xi}(s)e^{-i\omega t}$ and $\tilde{\xi}(s)$ is the purely spatial component of the tube displacement. The function ξ_\perp contains all of the scattering information that is needed to understand the interaction of the wave field with the flux tube.

2.3. Jacket Modes and a Lower Boundary

Bogdan & Cally (1995) showed that scattered waves created as a consequence of magnetic interactions are a mixture of modal and evanescent components. The scattering process results in not only a redistribution (and loss) of modal energies but also in the production of a continuous spectrum of evanescent “modes” called *jacket modes*. The existence of evanescent waves in the near field of an arbitrary scatterer (not just magnetic) that possesses subwavelength features has been well documented in the area of acoustics (e.g., Maynard et al. 1985) and optics (e.g., Bozhevolnyi & Vohnsen 1996). Mathematically, these evanescent modes appear to compensate for the inability of the set of propagating-mode eigenfunctions to represent a spatially intricate scatterer. These nonpropagating evanescent waves decay exponentially rapidly with distance from the scatterer.

The formalism of Bogdan & Cally (1995) requires an uncountable infinity of jacket modes to complete the basis, a consequence of the lower boundary being placed at $s = \infty$. Jacket modes in this instance are mathematically described using Whittaker functions, which are relatively difficult and expensive to compute accurately. Moreover, the jacket mode equations listed in Bogdan & Cally (1995) contain integrals over running indices that pose significant numerical hurdles because of the poor convergence properties of the integral. In order to circumvent any calculations involving these continuous jacket modes, we employ a lower boundary placed at a depth $s = D = 250$ ($z = 98 \text{ Mm}$) to reduce this uncountably infinite set of evanescent modes to a more tractable, discrete, countably infinite counterpart in the manner described in Barnes & Cally (2000).

Only modes whose inner turning points are in the vicinity of the lower boundary are affected by its presence, and therefore, placing it at a depth of 98 Mm means that the f - and first few p -modes remain unaware of its presence (because of the decay

of the eigenfunction). Moreover, the scattering amplitudes decrease sharply with increasing radial order. Consequently, the high-order p -modes which interact with the lower boundary are largely unimportant in any case because of their weak contribution to the scattering process studied here. With the introduction of the boundary, the problem becomes numerically well defined as well.

In order to obtain the p - and jacket mode eigenfunctions, we apply a zero Lagrangian pressure perturbation lower boundary condition for the sake of simplicity (see the appendix in Barnes & Cally 2000). We also assume that the tube oscillations (ξ_\perp in eq. [8]) are oblivious to the lower boundary. This condition is necessary because energy loss in the form of propagating Alfvén waves along the tube can only occur when the lower boundary is transparent (not the case with zero Lagrangian pressure perturbation).

To summarize, we use the formalism and model of Bogdan et al. (1996), but being unable to carry out calculations of the necessary jacket modes described in Bogdan & Cally (1995), we replace this uncommonly difficult continuous set of modes by its more tractable discrete cousin (Barnes & Cally 2000). Next, we describe the tube radius boundary condition that allows us to begin the task of estimating the scattering coefficients.

2.4. The Scattered Wave and Tube Boundary

The scattered wave is given by (e.g., Bogdan & Cally 1995)

$$\Psi_{\text{sc}} = - \sum_{n=0}^{\infty} \sum_{m=-\infty}^{\infty} i^m \left[\alpha_{mn}^p H_m^{(1)}(k_n^p r) \Phi_p(\kappa_n^p; s) + \beta_{mn}^j K_m(k_n^j r) \Phi_j(\kappa_n^j; s) \right] e^{i(m\theta - \omega t)}, \quad (9)$$

where α_{mn}^p are the p -mode scattering coefficients, β_{mn}^j are the jacket mode coefficients, and $K_m(w)$ is the K -Bessel function of order m and argument w . The resonant wavenumber of the p_n -mode is denoted by k_n^p (including the $n = 0$ f -mode), while wavenumbers corresponding to jacket modes are labeled k_n^j . The eigenvalues $\kappa_n^p > 0$ and κ_n^j are related to k_n^j and k_n^p , respectively, according to equation (5) (replace p by J in eq. [5]). In equation (3), the unnormalized jacket mode eigenfunction, $\Phi_j(\kappa_n^j; s)$, is given by

$$\Phi_j(\kappa_n^j; s) = s^{-1/2-\mu} \left[\eta_n^j M_{-i\kappa_n^j, \mu} \left(\frac{i\nu^2}{\kappa_n^j} s \right) + M_{-i\kappa_n^j, -\mu} \left(\frac{i\nu^2}{\kappa_n^j} s \right) \right], \quad (10)$$

where η_n^j , a parameter, and κ_n^j , the jacket mode eigenvalue, are determined by the boundary conditions (see Appendix A for details) and $M_{\kappa, \mu}(w)$ is the Whittaker function (Whittaker & Watson 1980). The normal to the tube boundary at a given depth s is given by

$$\hat{\mathbf{n}} = \frac{\hat{\mathbf{r}} - (1/z_0)(dR/ds)\hat{\mathbf{z}}}{\left\{ 1 + [(1/z_0)(dR/ds)]^2 \right\}^{1/2}}. \quad (11)$$

A consequence of the thin flux tube approximation is that $|dR/ds| \ll 1$; however, we retain this term throughout in order to verify that the scattering coefficients are at best weakly dependent on it (see § 3). The boundary condition is then obtained by matching radial velocities across the tube boundary, $r = R(s)$,

$$\hat{\mathbf{n}} \cdot \nabla (\Psi_{\text{inc}} + \Psi_{\text{sc}})_{r=R(s)} = \hat{\mathbf{x}} \cdot \hat{\mathbf{r}} \xi_\perp(s) e^{-i\omega t}, \quad (12)$$

where $\hat{\mathbf{x}}$ is the unit vector along the x -axis. Simplifying equation (12), we obtain

$$\left[\frac{\partial}{\partial r} (\Psi_{\text{inc}} + \Psi_{\text{sc}}) - \frac{1}{z_0^2} \frac{dR}{ds} \frac{\partial}{\partial s} (\Psi_{\text{inc}} + \Psi_{\text{sc}}) \right]_{r=R(s)} = e^{-i\omega t} \xi_\perp(s) \cos \theta \left[1 + \left(\frac{1}{z_0} \frac{dR}{ds} \right)^2 \right]^{1/2}. \quad (13)$$

Using a least squares approach, equation (13) is then solved to obtain an estimate for the scattering coefficients α_{mn}^p .

3. SOLUTION PROCEDURE

By only retaining the $|m| = 1$ coefficients and canceling the $e^{-i\omega t}$ term in equation (13), time and angular dependencies may be eliminated. Because we are only dealing with a single m , the scattering coefficients introduced in equation (9) are rewritten as α_n^p and β_n^j . We define the following functions

$$f(s) = \frac{i\xi_\perp(s)}{2} \sqrt{1 + \left(\frac{1}{z_0} \frac{dR}{ds} \right)^2} + \left(\frac{\partial}{\partial r} - \frac{1}{z_0^2} \frac{dR}{ds} \frac{\partial}{\partial s} \right) \times [J_1(k_0^p r) \Phi_p(\kappa_0^p; s)]_{r=R(s)}, \quad (14)$$

$$g_n^p(s) = \left(\frac{\partial}{\partial r} - \frac{1}{z_0^2} \frac{dR}{ds} \frac{\partial}{\partial s} \right) [H_1^{(1)}(k_n^p r) \Phi_p(\kappa_n^p; s)]_{r=R(s)}, \quad (15)$$

$$g_n^j(s) = \left(\frac{\partial}{\partial r} - \frac{1}{z_0^2} \frac{dR}{ds} \frac{\partial}{\partial s} \right) [K_1(k_n^j r) \Phi_j(\kappa_n^j; s)]_{r=R(s)}, \quad (16)$$

and arrive at the least-squares problem,

$$\mathbf{A} \begin{bmatrix} (\alpha) \\ (\beta) \end{bmatrix} = \begin{bmatrix} f(s_1) \\ \dots \\ f(s_M) \end{bmatrix}. \quad (17)$$

In equation (17), s_1 and s_M (M is the number of grid points in depth) are the start and end of the finite vertical domain, (α) and (β) are column vectors of the scattering coefficients α_n^p and β_n^j , and the $M \times (N_1 + N_2 + 1)$ matrix \mathbf{A} is given by

$$\mathbf{A} = \begin{bmatrix} g_0^p(s_1) & \dots & g_{N_1}^p(s_1) & g_1^j(s_1) & \dots & g_{N_2}^j(s_1) \\ \dots & \dots & \dots & \dots & \dots & \dots \\ g_0^p(s_M) & \dots & g_{N_1}^p(s_M) & g_1^j(s_M) & \dots & g_{N_2}^j(s_M) \end{bmatrix}, \quad (18)$$

where $N_1 + 1$ and N_2 are the number of p - and jacket modes included in this calculation, respectively. The grid spacing in the s -space was set at $\Delta s = 0.249$ or, correspondingly, $\Delta z = 97$ km. For physical parameters, we utilize the model described in Bogdan et al. (1996) wherein $m = 1.5$, $\Phi = 3.88 \times 10^{17}$ Mx, $R(s = 1) = 100$ km, $z_0 = 392$ km, and incident modes of frequency, $\omega = 2\pi\nu$, $\nu = 2, 3, 4, 5$ mHz, and $\beta = 0.1, 1, 10$. The lower boundary of the box is set at $D = 250$ or 98 Mm. The thin flux tube approximation may be invoked to ignore the dependence of various terms on derivatives with respect to s in this calculation. Although not shown here, we verified the validity of this approximation by demonstrating the invariance of the scattering coefficients to the presence of the derivative terms. That the derivative terms contribute very little to the solution is an important test of the thin flux tube approximation. In addition,

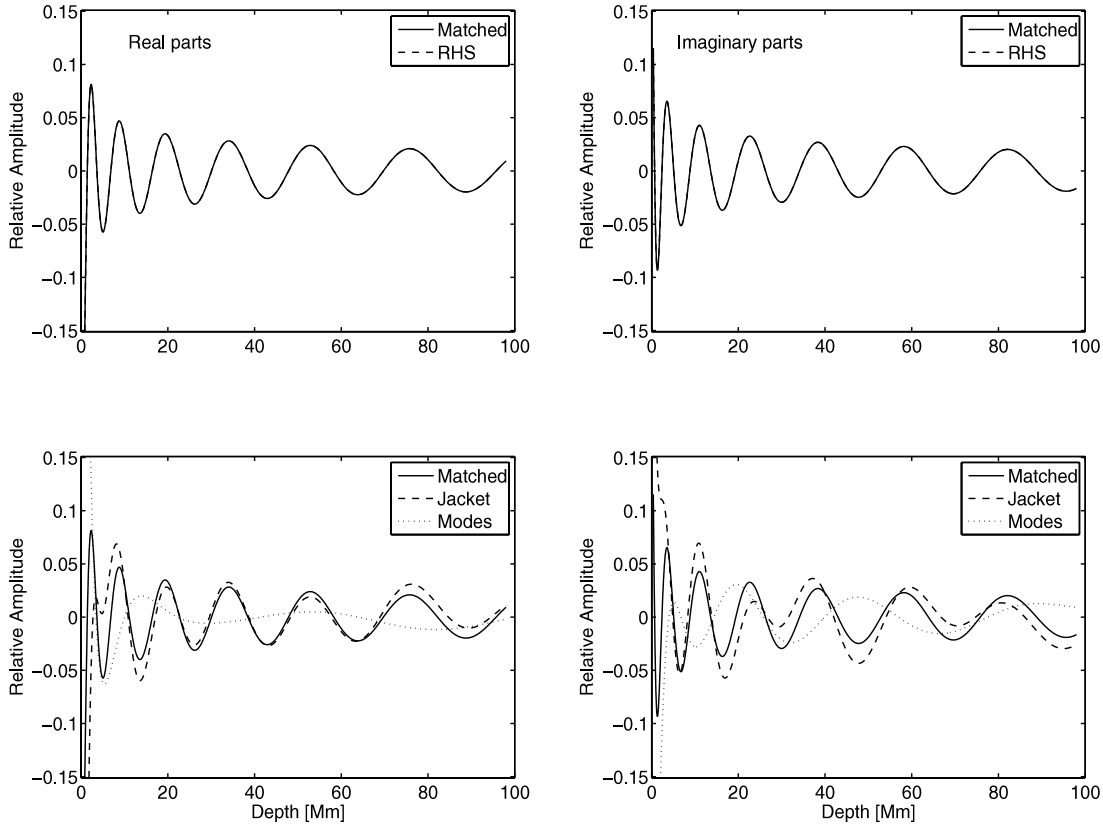


FIG. 1.— *Top*: Comparisons of real and imaginary parts of the fit (labeled “matched” in the figure) to the corresponding real and imaginary parts of the right-hand side ($=f(s)$, eq. [14]) for $\beta = 1$ and $\nu = 3$ mHz. The curves are indistinguishable. *Bottom*: Contributions to the real and imaginary parts of the right-hand side, respectively, from the jacket and resonant modes. The lower boundary was placed at a depth of 98 Mm; the surface gravity mode with eight normal and 675 jacket modes were used in this matching. The scattered amplitude is normalized with respect to the incident f -mode amplitude.

we considered a near-field approximation of the terms $J_1(k_0^p r)$, $H_1^{(1)}(k_n^p r)$, and $K_1(k_n^j r)$ in equations (14)–(16). Applying this approximation to J and H does not significantly change our solutions. However, the near-field approximation to the Bessel K leads to substantially different solutions for the scattering coefficients.

The coefficients for the first four modes were seen to be stable to changes in the depth of the lower boundary, as discussed in § 2.3. To test the accuracy of the p -mode scattering coefficients, we attempted to match the energies of the ingoing with the outgoing and Alfvén waves. However, because their amplitudes are so low, we find that small changes in the phase of the scattered f -mode result in significant changes in the amplitudes of the high-order scattered p -modes. This implies a lack in the robustness of the result; hence, we only show the values of the f - and p_1 -mode scattering coefficients.

Large numbers of jacket modes (463, 675, 820, and 857 for $\nu = 2, 3, 4$, and 5 mHz, respectively) are required to fit the right-hand side with the accuracy of Figure 1. Least-squares fitting was performed using the backslash command in MATLAB. The various complementary and standard Whittaker functions were computed using CERNLIB, a freely available suite of mathematical functions. The absolute values of a sample of the scattering coefficients $|\alpha_n^p|$ and corresponding phases $\arg(\alpha_n^p)$ for plasma- $\beta = 1$ and $\nu = 3$ mHz are listed in the second and third columns of Table 1. We do not display the jacket mode coefficients here.

Our confidence in these values is strengthened by the consistency in the values of the scattering coefficients over a large number of numerical experiments. We show in the top row of Figure 1 that the combination of resonant and jacket modes captures the right-hand side very well. In the bottom row, the

contributions of the jacket and resonant modes are separated to illustrate that jacket modes are a nontrivial component of the scattering process. Shown in Figure 2 is the agreement with intuitive expectation that the higher the radial order of the p -mode, the lower the contribution. This is in line with the idea of a diagonally dominant scattering matrix (for scattering matrix see, e.g., Braun 1995)—i.e., a scattering matrix with weak off-diagonal terms that decay very rapidly.

There is a definite dependence of the magnitude of the scattering coefficients on the plasma- β and the frequency of the incident wave (e.g., Bogdan et al. 1996). It emerges from our calculations that the wave-flux tube coupling becomes stronger as the frequency increases (see Fig. 2). Moreover, as the flux tube becomes magnetically dominated ($\beta = 0.1$), the scattering is enhanced, as emphasized by the magnitudes of the scattering coefficients. Correspondingly, the flux tube becomes relatively stiff and the tube kink mode is more resistant to the buffeting forces of the interacting modes (Fig. 3, *top*). The reverse effect is observed for $\beta = 10$, where the tube is hydrodynamically dominated (Fig. 3, *bottom*). In addition, the scattering coefficients

TABLE 1
SCATTERING COEFFICIENTS FOR $\beta = 1$ AND $\nu = 3$ mHz
FOR A FLUX TUBE WITH RADIUS 100 km AT $s = 1$

Mode	Amplitude	Phase (deg)
f	0.0117	49.6
p_1	0.0007	76.7

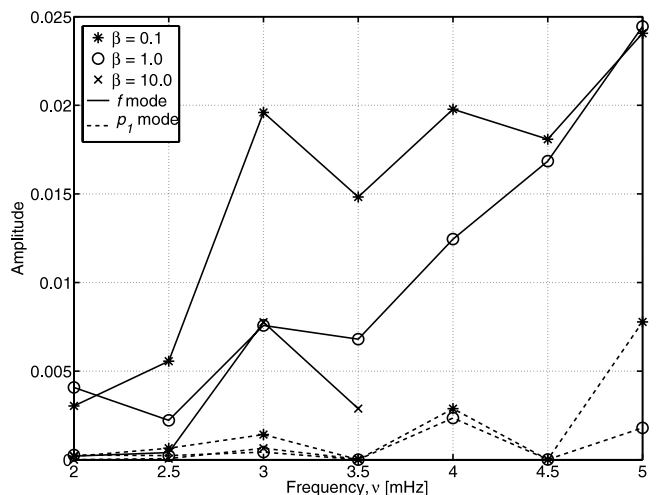


FIG. 2.—Amplitudes of the scattered f - (solid lines) and p_1 -modes (dashed lines) at various values of plasma- β and frequency, ν . The p_1 scattering coefficients are seen to be substantially smaller than the corresponding ones for the f -mode.

increase nonlinearly with the amount of flux (and therefore tube radius) at fixed β and ν . Since the thin flux tube approximation requires that the tube radius at the surface be smaller than a scale height, we can only study a restricted set of radii (see Fig. 4).

4. CONCLUSIONS

We have presented a model of wave scattering off a magnetic flux concentration. Earlier efforts to model magnetoacoustic interactions (e.g., Gizon et al. 2006) have been under less realistic conditions because of the related mathematical difficulties. However, it is noted that this model does not capture the complexities of the solar case where phenomena such as radiative heat transfer, azimuthal asymmetries in the tube, the lack of applicability of the thin tube approximation in near-surface regions, local changes in source properties, downflows, etc., probably play an important role in affecting the wave field. Even under

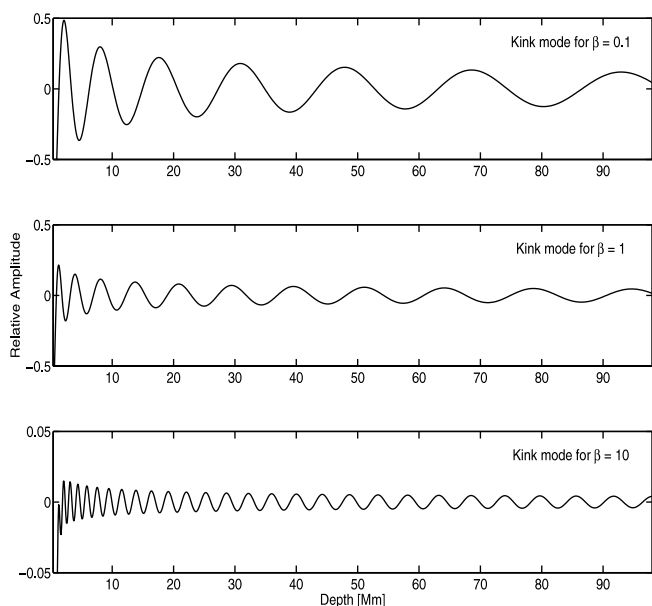


FIG. 3.—Kink modes at $\nu = 5$ mHz for different values of β . The magnetically dominated case with $\beta = 0.1$ is seen to be very stiff, as opposed to the $\beta = 10$ case. The amplitude of the mode is normalized by the amplitude of the incoming f -mode. [See the electronic edition of the Journal for a color version of this figure.]

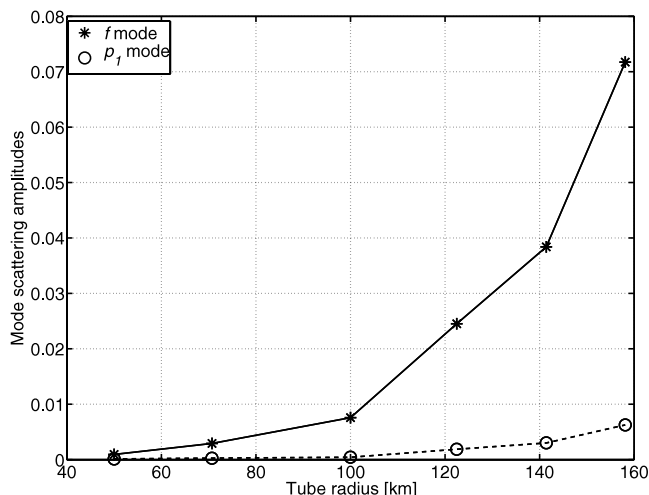


FIG. 4.—Scattering coefficients for $\nu = 3$ mHz and $\beta = 1$ as a function of tube radius. The flux $\Phi \propto R^2$, where R is the tube radius. A clear trend with increasing tube radius (or flux) is seen. The thin flux tube approximation requires the tube radius to be smaller than a scale height (≈ 260 km); therefore, we cannot study the scattering at large values of R .

relatively idealized conditions as in this model, the manipulations required to recover the scattering properties are nontrivial. Perhaps this indicates that the formalism is suboptimal when keeping in mind the relatively significant effort required to compute in this basis set of Whittaker functions while coping with the restricted generality of the solutions. With the development of methods of computational forward modeling to address issues of wave interactions with magnetic fields (e.g., Cameron et al. 2007; Hanasoge 2008) comes the ease of studying these problems in greater generality. The estimates for the degree of scattering obtained here can be used to test the validity of numerical forward calculations.

It is shown that the contribution to the scattering process by the so-called *jacket* or evanescent modes is entirely nontrivial and, therefore, inevitable in studies of scatterers that contain subwavelength variations in their spatial structure. It has been realized by Maynard et al. (1985) that these near-field evanescent modes may be analyzed to image with subwavelength resolution. Thus, future prospects of studying these flux tubes in greater detail are exciting, especially in the context of upcoming satellite missions.

Lastly, to say something about the nature of the average flux tube in the measurements of Duvall et al. (2006) based on this analysis, we first assume that the interactions are well captured by the single scattering approximation. This implies that the scattering magnitude will scale linearly with the number of model flux tubes while the phase of the scattered wave is unchanged from the value listed in Table 1. While our scattering model overestimates the amplitude of scatter by a factor of 8.8, the phase of the f -mode scattering coefficient agrees well with the observations. Several possibilities arise: either the $\beta \gg 1$ for flux tubes in the Sun, or the upper boundary conditions of this model are inaccurate, or there are important pieces of physics, like nonlinearities, radiative heat transfer, etc., not accounted for here. More conclusive results await further investigations.

S. M. H. was funded by NASA grants MDI NNG 05-GH14G and HMI NAS 5-02139. Computations were performed on the Stanford Solar group machines.

APPENDIX A

EIGENVALUES

A1. JACKET MODE EIGENVALUES

The functional form of jacket modes used in our calculations is given by equation (10). These functions are forced to satisfy the boundary conditions

$$\frac{\partial \Phi_J}{\partial s} + \frac{\nu^2}{m} \Phi_J = 0 \quad (\text{A1})$$

at $s = 1$ and D . Defining

$$N_J(\kappa_n^J, \mu, s) = \frac{1/2 + \mu}{s} M_{-i\kappa_n^J, -\mu} \left(\frac{i\nu^2}{\kappa_n^J} s \right) - \frac{i\nu^2}{\kappa_n^J} M'_{-i\kappa_n^J, -\mu} \left(\frac{i\nu^2}{\kappa_n^J} s \right) - \frac{\nu^2}{m} M_{-i\kappa_n^J, -\mu} \left(\frac{i\nu^2}{\kappa_n^J} s \right), \quad (\text{A2})$$

$$D_J(\kappa_n^J, \mu, s) = -\frac{1/2 + \mu}{s} M_{-i\kappa_n^J, \mu} \left(\frac{i\nu^2}{\kappa_n^J} s \right) + \frac{i\nu^2}{\kappa_n^J} M'_{-i\kappa_n^J, \mu} \left(\frac{i\nu^2}{\kappa_n^J} s \right) + \frac{\nu^2}{m} M_{-i\kappa_n^J, \mu} \left(\frac{i\nu^2}{\kappa_n^J} s \right), \quad (\text{A3})$$

the eigenvalues κ_n^J are determined through the relation

$$N_J(\kappa_n^J, \mu, 1) D_J(\kappa_n^J, \mu, D) = N_J(\kappa_n^J, \mu, D) D_J(\kappa_n^J, \mu, 1). \quad (\text{A4})$$

Subsequently, the constant η_n^J in equation (10) is obtained,

$$\eta_n^J = \frac{N_J(\kappa_n^J, \mu, 1)}{D_J(\kappa_n^J, \mu, 1)} = \frac{N_J(\kappa_n^J, \mu, D)}{D_J(\kappa_n^J, \mu, D)}. \quad (\text{A5})$$

A2. p -MODE EIGENVALUES

The functional form of p -modes, given by equation (4), has to satisfy

$$\frac{\partial \Phi_p}{\partial s} + \frac{\nu^2}{m} \Phi_p = 0, \quad (\text{A6})$$

at $s = 1$ and D . Following the formalism of Appendix A.1, we define N_p and D_p as

$$N_p(\kappa_n^p, \mu, s) = \frac{1/2 + \mu}{s} M_{\kappa_n^p, -\mu} \left(\frac{\nu^2}{\kappa_n^p} s \right) - \frac{\nu^2}{\kappa_n^p} M'_{\kappa_n^p, -\mu} \left(\frac{\nu^2}{\kappa_n^p} s \right) - \frac{\nu^2}{m} M_{\kappa_n^p, -\mu} \left(\frac{\nu^2}{\kappa_n^p} s \right), \quad (\text{A7})$$

$$D_p(\kappa_n^p, \mu, s) = -\frac{1/2 + \mu}{s} M_{\kappa_n^p, \mu} \left(\frac{\nu^2}{\kappa_n^p} s \right) + \frac{\nu^2}{\kappa_n^p} M'_{\kappa_n^p, \mu} \left(\frac{\nu^2}{\kappa_n^p} s \right) + \frac{\nu^2}{m} M_{\kappa_n^p, \mu} \left(\frac{\nu^2}{\kappa_n^p} s \right), \quad (\text{A8})$$

and determine the eigenvalue κ_n^p and constant ζ_n^p in equation (4), respectively, through the following relations,

$$N_p(\kappa_n^p, \mu, 1) D_p(\kappa_n^p, \mu, D) = N_p(\kappa_n^p, \mu, D) D_p(\kappa_n^p, \mu, 1), \quad (\text{A9})$$

$$\zeta_n^p = \frac{N_p(\kappa_n^p, \mu, 1)}{D_p(\kappa_n^p, \mu, 1)} = \frac{N_p(\kappa_n^p, \mu, D)}{D_p(\kappa_n^p, \mu, D)}. \quad (\text{A10})$$

APPENDIX B

DETERMINING THE AMPLITUDE AND PHASE OF THE SCATTER FROM OBSERVATIONS

Through analyses of Michelson Doppler Imager (MDI) data (Scherrer et al. 1995) and the application of the forward models of Gizon & Birch (2002), Duvall et al. (2006) estimated the complex scattering amplitude (d in their paper) due to network magnetic elements. Assume an incident plane wave of the form, i.e., an alternate form of equation (3),

$$\Phi^{\text{in}} = e^{ik_0^p x - i\omega t} \Phi_p(k_0^p; s), \quad (\text{B1})$$

where $x = \hat{\mathbf{x}} \cdot \mathbf{r}$, with the velocity of the wave given by

$$\mathbf{v}_h^{\text{in}} = \frac{\partial}{\partial t} \nabla \Phi^{\text{in}} = \omega \mathbf{k} \Phi^{\text{in}}. \quad (\text{B2})$$

For dipole scattering only, the scattered f -mode takes on the form

$$\Phi^{\text{sc}} = -2i\alpha_{10}^p \cos \theta H_1^1(k_0 r) \Phi_p(k_0^p; s). \quad (\text{B3})$$

Using conventions from Gizon & Birch (2002) and the definition of dipole scattering of Duvall et al. (2006), we have

$$\mathcal{L}_0 \delta v_z = -\delta \mathcal{L} \mathbf{v}^{\text{in}} = -\nabla_h \cdot (d \mathbf{v}_h^{\text{in}}). \quad (\text{B4})$$

Solving equation (B4) for a point scatterer,

$$\delta v_z(\mathbf{r}, \omega) = -2\pi \int d\mathbf{s} G_z(\mathbf{r} - \mathbf{s}, \omega) \nabla_s \cdot [d \delta(\mathbf{s}) \mathbf{v}_h^{\text{in}}(\mathbf{s}, \omega)], \quad (\text{B5})$$

which upon integrating by parts produces

$$\delta v_z(\mathbf{r}, \omega) = 2\pi d \int d\mathbf{s} \delta(\mathbf{s}) \mathbf{v}_h^{\text{in}}(\mathbf{s}, \omega) \cdot \nabla_s G_z(\mathbf{r} - \mathbf{s}, \omega), \quad (\text{B6})$$

or

$$\delta v_z(\mathbf{r}, \omega) = -2\pi d \mathbf{v}_h^{\text{in}}(0, \omega) \cdot \nabla_r G_z(\mathbf{r}, \omega). \quad (\text{B7})$$

In the far field, the Green's function reduces to

$$G_z(\mathbf{r}) \approx \frac{i}{4\pi g} H_0^1(k_0 r). \quad (\text{B8})$$

The derivative in equation (B7) becomes

$$\nabla_r G_z(\mathbf{r}) \approx -\frac{ik}{4\pi g} H_1^1(k_0 r) \hat{\mathbf{r}}, \quad (\text{B9})$$

and equation (B7) along with the expression for the wave velocity from equation (B2) simplifies to

$$\delta v_z(\mathbf{r}, \omega) = \Psi_p(k_0^p; s) \frac{i\omega k^2 d}{2g} H_1^1(k_0 r) \cos \theta, \quad (\text{B10})$$

and therefore,

$$\Phi^{\text{sc}} = \delta \Phi = \frac{\delta v_z}{-ik\omega} = -\frac{kd}{2g} \cos \theta H_1^1(k_0 r) \Phi_p(k_0^p; s). \quad (\text{B11})$$

From equation (B3), we obtain the following scattering coefficient,

$$\alpha_{10}^p = -\frac{ik}{4g} d \quad (\text{B12})$$

For d with a phase of about 130° (Duvall et al. 2006), α_{10}^p has a phase of about 40° .

REFERENCES

- Barnes, G., & Cally, P. S. 2000, *Sol. Phys.*, 193, 373
 Bogdan, T. J. 1989, *ApJ*, 345, 1042
 Bogdan, T. J., & Cally, P. S. 1995, *ApJ*, 453, 919
 Bogdan, T. J., Hindman, B. W., Cally, P. S., & Charbonneau, P. 1996, *ApJ*, 465, 406
 Bozhevolnyi, S. I., & Vohnsen, B. 1996, *Phys. Rev. Lett.*, 77, 3351
 Braun, D. C. 1995, *ApJ*, 451, 859
 Cameron, R., Gizon, L., & Daifallah, K. 2007, *Astron. Nachr.*, 328, 313
 Cattaneo, F. 1999, *ApJ*, 515, L39
 Cheung, M. C. M., Moreno-Insertis, F., & Schüssler, M. 2006, *A&A*, 451, 303
 Crouch, A. D., & Cally, P. S. 1999, *ApJ*, 521, 878
 Duvall, T. L., Jr., Gizon, L., & Birch, A. C. 2006, *ApJ*, 646, 553
 Duvall, T. L., Jr., Jeffries, S. M., Harvey, J. W., & Pomerantz, M. A. 1993, *Nature*, 362, 430
 Gizon, L., & Birch, A. C. 2002, *ApJ*, 571, 966
 Gizon, L., Hanasoge, S. M., & Birch, A. C. 2006, *ApJ*, 643, 549
 Hanasoge, S. M. 2008, *ApJ*, in press
 Maynard, J. D., Williams, E. G., & Lee, Y. 1985, *J. Acoustical Soc. Am.*, 78, 1395
 McIntosh, S. W., Fleck, B., & Judge, P. G. 2003, *A&A*, 405, 769
 McIntosh, S. W., & Jeffries, S. M. 2006, *ApJ*, 647, L77
 Scherrer, P. H., et al. 1995, *Sol. Phys.*, 162, 129
 Spruit, H. C. 1981, *A&A*, 102, 129
 Spruit, H. C., & Bogdan, T. J. 1992, *ApJ*, 391, 109L
 Whittaker, E. T., & Watson, G. N. 1980, *A Course of Modern Analysis* (Cambridge: Cambridge Univ. Press)